Journal of Materials Processing Technology 229 (2016) 313–321

Contents lists available at ScienceDirect

Journal of Materials Processing Technology

journal homepage: www.elsevier.com/locate/jmatprotec

Optimizing tool diameter for friction stir welded brass/steel lap joint

Y. Gao[a,b,*], K. Nakata[a], K. Nagatsuka[a], Y. Shibata[c], M. Amano[c]

[a] Joining and Welding Research Institute, Osaka University, Ibaraki 567-0047, Japan
[b] Kurimoto Ltd., 2-8-45 Suminoe, Osaka 559-0021, Japan
[c] Komatsu Ltd., 3-1-1 Ueno, Hirakata-shi, Osaka 573-1011, Japan

ARTICLE INFO

Article history:
Received 18 September 2014
Received in revised form
14 September 2015
Accepted 15 September 2015
Available online 18 September 2015

Keywords:
Brass
Steel
Dissimilar joint
Tool diameter
Diffusion

ABSTRACT

A 3.0-mm-thickness brass plate used as a top plate, was lap jointed to a 5.0-mm-thickness structural steel bottom plate by friction stir welding. Five kinds of tools with different probe and shoulder diameters were used in this study. The effect of tool diameter on microstructure and mechanical properties of the joints was studied. Grain size at the stirred zone, tensile shear fracture load and the tensile shear strength of the joints varied significantly with tool diameter. A mutual diffusion zone of dominant elements of each plate was found at the joint interface.

1. Introduction

Brass (Cu–Zn alloy) has good features such as higher plasticity, strength, hardness and corrosion resistance than pure copper, therefore it has been applied as structural materials in the industry. In recent years, European Union Regulation of REACH restricted the use of materials containing lead as alloying element, such as lead bronze. Therefore, brass has been used as the replacement of lead bronze to produce the sliding parts of hydraulic equipment to obtain good tribological property. For sliding parts, hybrid structures of brass/steel dissimilar metal joint are preferred as it requires higher structural strength at a lower cost. However, it is very difficult to clad brass to steel by fusion welding because of the strength loss in the fusion zone due to the evaporation of Zn, as well as the large differences in the thermal physical properties between brass and steel, such as melting point, thermal conductivity and thermal expansion coefficient.

To solve this problem, friction welding as a solid-state welding process has been tried in recent years. Luo et al. (2012) used the CT-130 type special inertia friction welding machine to finish the H90 brass /high carbon steel dissimilar metals radial friction welding process and Kimura et al. (2010) achieved the brass/low carbon steel dissimilar metal welding by friction welding. However, the friction welding has a large limitation in the shape of the joint, which should be a body of rotation such as a pipe and a rod-type joint.

Friction stir welding (FSW), a novel solid-state welding process developed by The Welding Institute (TWI), can weld plate-shaped materials as butt or lap joints with large applicability in the dimension of the joint. In early years, FSW was introduced for light alloys such as Al alloys. Recently, high performance tool materials are employed for FSW of high melting temperature materials such as titanium, nickel and steels (Nandan et al., 2008). In addition, FSW also has been used for joining dissimilar metals, such as Al alloy/steel (Chen and Nakata., 2008), Mg alloy/steel (Chen and Nakata., 2010), Al alloy/copper (Galvao et al., 2013) and Ti/steel (Liao et al., 2010). For the brass/steel joint by FSW, only the Matsuyama et al. (2013) achieved the parametric study on the 64brass/steel lap joints by FSW to make clear the process window.

For increasing the binding strength of FSW lap joints, enlarge the joint width by increasing the diameter of FSW tool is the most direct method. Several researches have examined the effect of tool dimensions on FSW quality for the butt joint. Reynolds and Tang (2007) used several different variations of cylindrical probes with a concave shoulder to show that defect-free friction stir welds in 8.1 mm thick 2195 aluminum alloys could be produced with the probe diameter-to-shoulder diameter ratio between 2 to 1 and 3.125 to 1. Peel et al. (2003) evaluated cylindrical probes with either a standard metric M5 thread (5 mm wide with 0.8 mm pitch) or a

* Corresponding author at: Kurimoto Ltd., 2-8-45 Suminoe, Osaka 559-0021, Japan.
E-mail address: y_gao@kurimoto.co.jp (Y. Gao).

http://dx.doi.org/10.1016/j.jmatprotec.2015.09.029
0924-0136/

Table 1
Nominal chemical composition of brass and S25C (mass%).

Alloy	Chemical composition (mass%)									
	C	Si	P	S	Cr	Mn	Fe	Ni	Cu	Zn
Brass	–	–	–	–	–	–	–	–	61	Rem.
S25C	0.25	0.28	0.02	0.01	0.18	0.52	Rem.	0.07	0.14	–

wider probe (6 mm wide) with a coarser thread (1 mm pitch). At higher travel speed (200 mm/min), the broader 6 mm tool with the coarser threads was more effective in disrupting the faying interface between the two joined workpieces. This change of probe design produced a 16% increase in joint efficiency. However, the study on the effect of tool diameter on FSW lap joint has not been made up to now.

In this study, the dissimilar lap joints of brass/steel were welded by FSW with constant welding parameters but five kinds of tools with different probe and shoulder diameters. The effect of tool diameter on microstructure and mechanical properties of the joints was studied.

2. Experimental details

Plates of commercially available brass ($3 \times 100 \times 200\,mm^3$) and plain carbon steel (S25C, $5 \times 100 \times 200\,mm^3$) were subjected to FSW, with brass used as the top plate and S25C as the substrate plate (Fig. 1). Table 1 shows the nominal chemical compositions of these materials. The WC-Co based FSW tools comprises of a concave shoulder of 15 and 20 mm in diameter, different probe diameters of 6, 8 and 10 mm but the constant probe length of 2.9 mm. The probe length is 0.1 mm shorter than the thickness of top brass plate (3 mm). The dimensions of five kinds of tools are shown in Table 2 and probe diameter (PD) to shoulder diameter (SD) ratios ranged from 2.5 to 1.5. The pictures of the FSW tools are shown in Fig. 2. Fig. 2(a) shows the schematic diagram of FSW tool, Fig. 2(b) shows the appearance of tool before FSW (SD:15 mm, PD:10 mm), Fig. 2(c) shows the appearances of five kinds of tools after FSW. There is no abrasion but only a very thin layer of brass on the shoulder

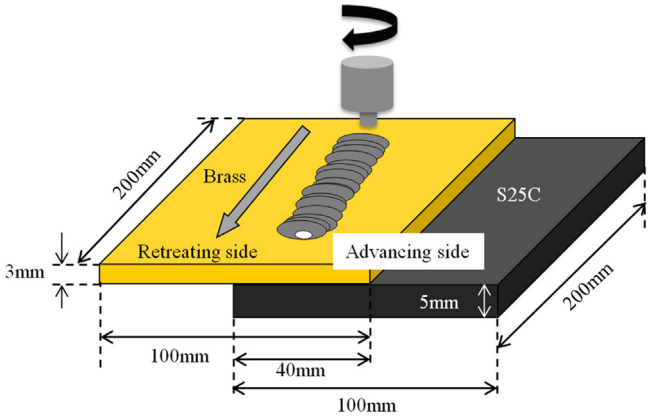

Fig. 1. Schematic diagram of the geometry of a dissimilar brass/S25C lap design.

Table 2
The dimensions of five kinds of tools which were used in this study.

	Shoulder diameter SD (mm)	Probe diameter PD (mm)	Shoulder to probe ratio SD:PD
(1)	15	6	2.5:1
(2)	15	8	1.9:1
(3)	15	10	1.5:1
(4)	20	8	2.5:1
(5)	20	10	2:1

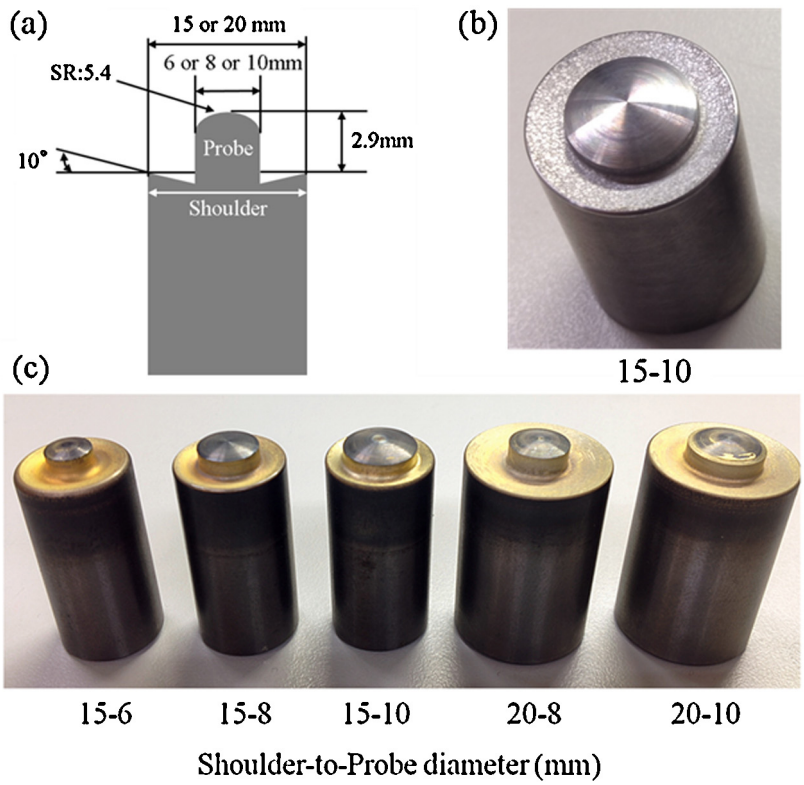

Fig. 2. The pictures of FSW tools. (a) Schematic diagram of tool, (b) the appearance of tool before FSW (SD:15 mm, PD:10 mm), (c) the appearances of five kinds of tools after FSW.

was observed after FSW. Lap joints were performed with the constant FSW parameters of the tool rotation rate of 1000 rpm, welding speed of 500 mm/min and load of 9.8 kN with a tool title angle of 3°, which are decided by preliminary experiments (Matsuyama et al., 2013).

The FSW joints were cross-sectioned perpendicular to the welding direction using an electrical-discharge cutting machine for metallographic analysis and tensile shear test. The specimens were prepared for optical microscopy by polishing and then etching with an acid solution of 20 mL HCl, 100 mL ethanol and 5 g $FeCl_3$. The microstructures of the joints were studied using optical microscopy (OM), scanning electron microscopy (SEM) and transmission electron microscopy (TEM). The grain sizes of the α-phase in the brass stirred zone (SZ) near the interfaces were measured using the line-intercept method, where the mean grain widths of α-phase on all the 10 lines drawn onto the SEM image magnified by 3000× for each welded joint are measured. The microhardness profile measurements was conducted on the cross-section of the lap joints using a microvickers hardness tester under a load of 0.1 N and a holding time of 15 s at the brass side 0.5 mm from the interface. Element distributions and chemical compositions of the joint interface were analyzed using an energy-dispersive X-ray spectrometer (EDX) equipped with an SEM or TEM. In addition, the specimens for shear tensile test (15 × 160 mm) were machined from the joints, and shear tensile test was performed at room temperature with a constant crosshead speed of 1 mm/min. The fractography of the tensile fracture surfaces is discussed using SEM and EDX investigations.

3. Results and discussion

3.1. Macro and microstructures in joints

Fig. 3 displays the brass surface appearances of the FSW joints welded by five kinds of tools. All of the joints are sound. Fig. 4 shows the macrostructures (OM) of the joints and higher magnified microstructure of the interfaces (SEM). Mean grain size of the α-phase in brass SZ of the joints are shown in the bottom of each photo. The brass metal has the microstructure consisted of two phases, α and β, which approved as convex and concave phases in SEM photos, respectively. As the increase of PD or SD, SZ of the joints became larger, which resulted in the increase of the joint width at the interfaces. The increase of PD can enlarge the SZ directly and the increase of SD can assist the plastic flow of brass by enhancing the thermal input. Near the joint interfaces, grain size of the

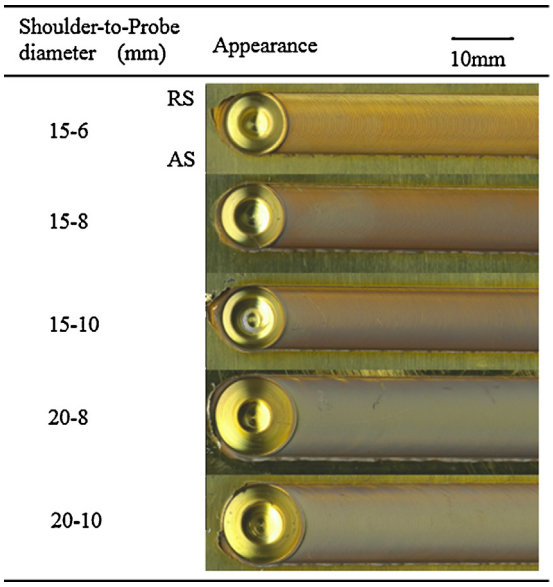

Fig. 3. Bead appearances of the joints welded with different tools.

α-phase became larger with the increase of PD or SD. It means that as the increase of PD or SD, the thermal input increased during FSW processing. SD has greater influence than PD for the change of the grain size of α-phase. Fig. 5 shows the distributions of Cu, Zn and Fe elements near the interface of the joint with SD of 20 mm and PD of 10 mm. A flat and no-cavity interface was observed macroscopically. It means that the tip of probe did not insert into the steel substrate.

3.2. Hardness in joints

Vickers hardness distributions across the joints welded by the different PD are shown in Fig. 6(a). The hardness in SZ is higher than that in brass base metal in each case because of grain refinement, but decreased with increasing PD because of the increase of grain size in SZ. For the same reason, the hardness value also decreased with increasing SD as shown in Fig. 6(b). It is well known that for conventional polycrystals with grain size ranging from several to hundreds of micrometers, the hardness dependence on the mean grain size can be descried by the Hall–Petch relation, $HV = HV_0 + kd^{-1/2}$, where HV is the hardness of a polycrystalline metal, d is the grain size and HV_0 and k are constants. The

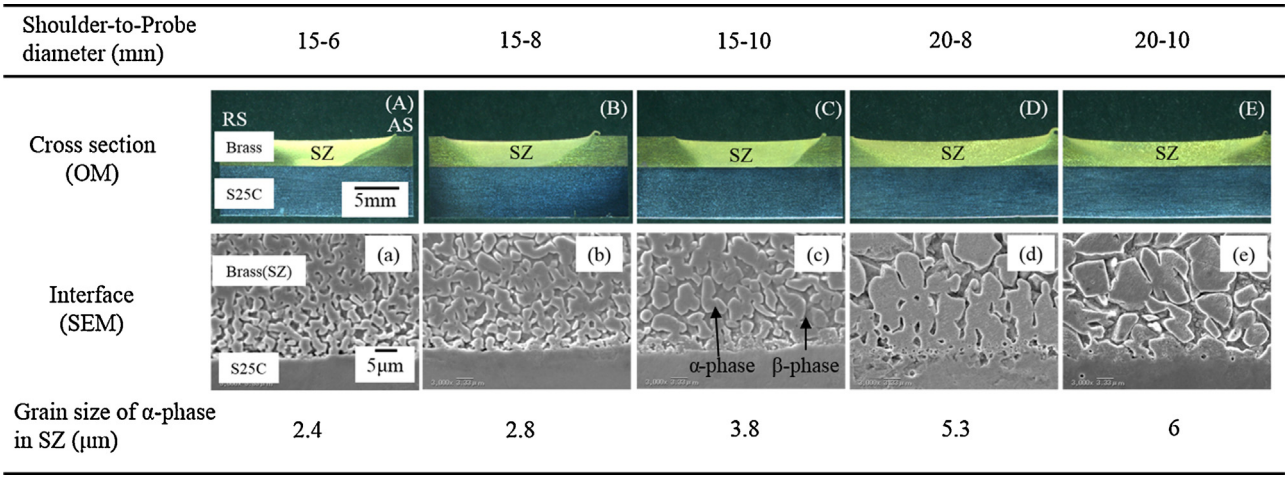

Fig. 4. Cross-sections and interface microstructures of the lap joints with constant welding parameters but different tools.

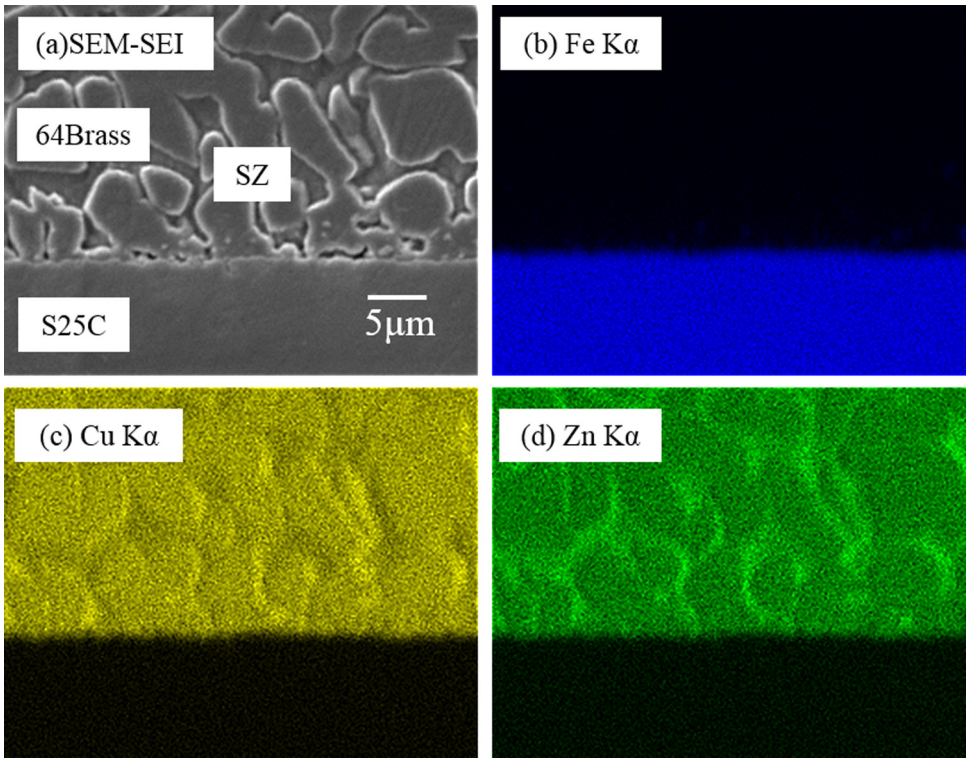

Fig. 5. The distribution of element near the interface with SD 20 mm and PD 10 mm, (a) SEM micrograph of the interface, (b) Fe, (c) Cu, (d)Zn area maps, respectively.

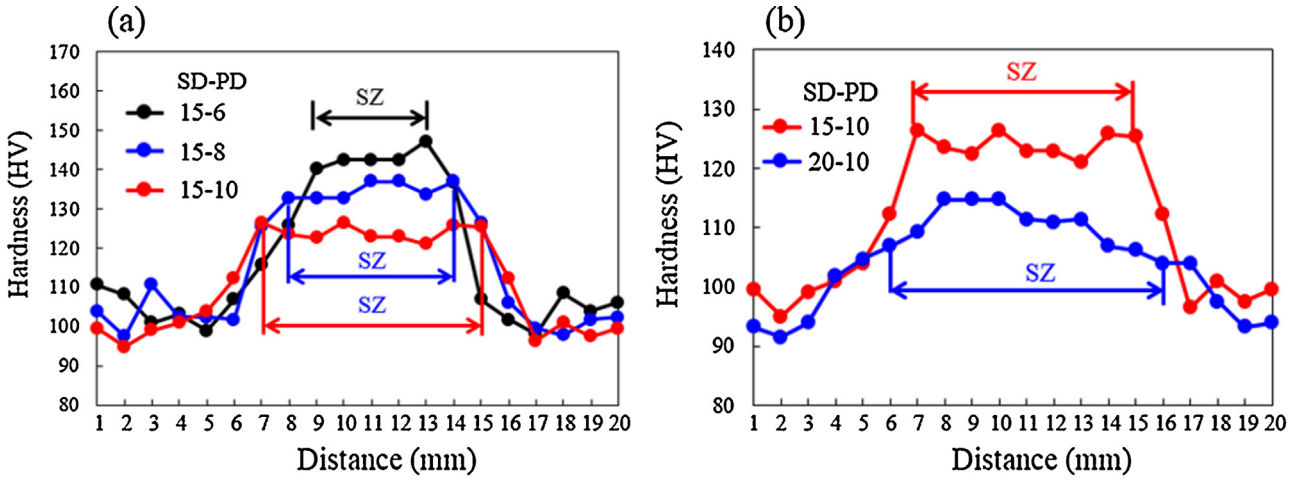

Fig. 6. Typical hardness profiles on the cross section of the lap joints welded with different tools. (a) The same SD but different PD, (b) the same PD but different SD.

Hall–Petch relation predicts an increased hardness with a decrease in the grain size (Fujii et al., 2010). In this study, grain size of the α-phase fell on the straight lines representing the Hall–Petch relation as shown in Fig. 7.

3.3. Formation mechanism of the interface

In order to clarify the formation mechanism of the interface between brass and S25C, the TEM sample across the joint interface was prepared by a focused ion beam (FIB) instrument. Fig. 8(a) shows TEM bright field image (BFI) for the interface of the joint with SD 15 mm and PD 10 mm (the joint got the best tensile shear fracture load which introduced in Section 3.4). Fig. 8(b) shows the higher magnification TEM micrograph of the square position 1 in Fig. 8(a). The distributions of Fe, Cu and Zn elements in the position 1 as shown in Fig. 8(c)–(e), respectively, indicates that some

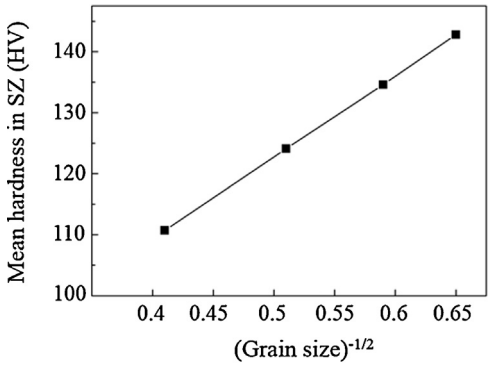

Fig. 7. Relationship between the hardness and the $(\text{grain size})^{-1/2}$ of α-phase in the SZ.

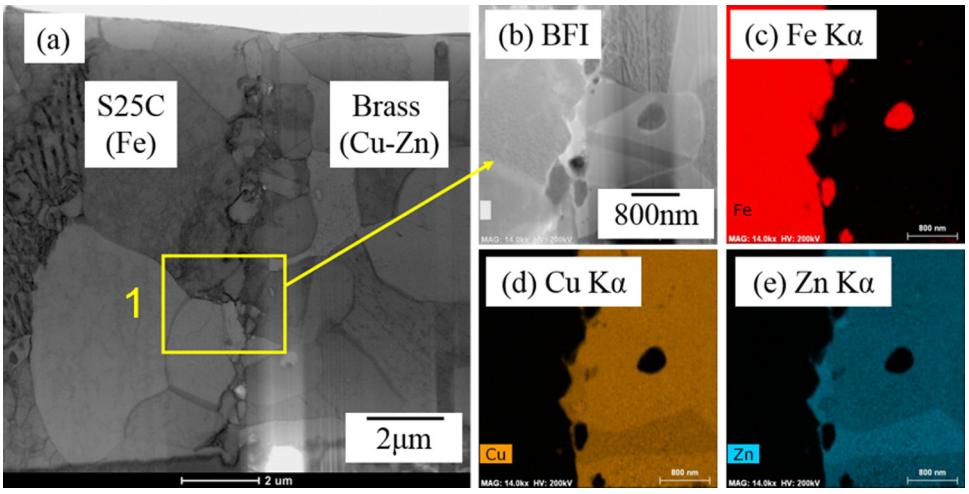

Fig. 8. Element mapping at the interface of the joint with SD 15 mm and PD 10 mm, (a) TEM bright field image of the interface, (b) the higher magnified TEM bright field image, (c) Fe, (d) Cu, (e) Zn area maps, respectively.

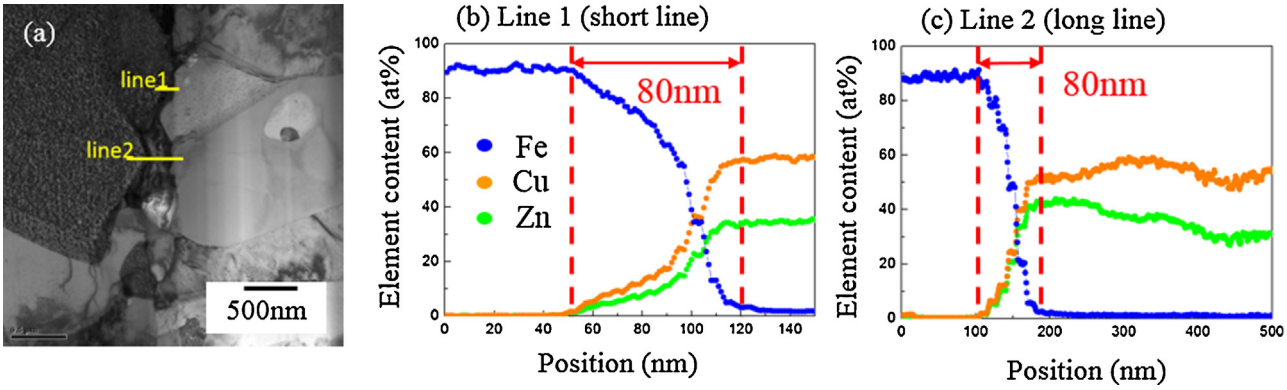

Fig. 9. Results of line analysis of Fe, Cu and Zn across the interface, (a) TEM bright field image of the interface, and results of line analysis of line 1 (b) and line 2 (c).

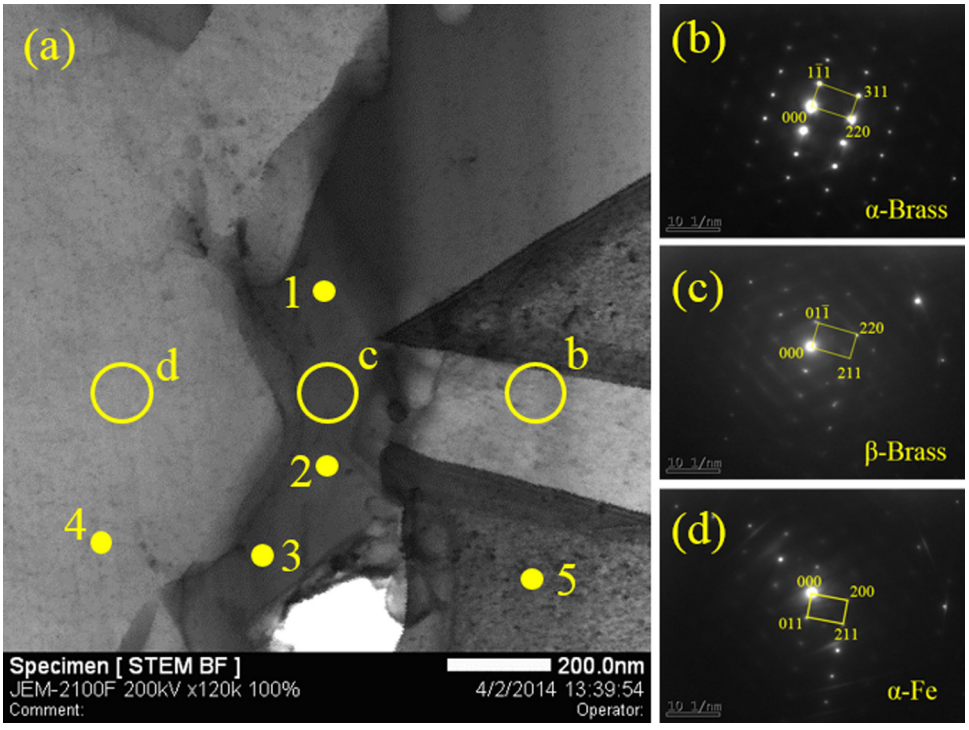

Fig. 10. TEM bright field image of the intermixed interface (a) and the selected area diffraction patterns of positions b, c and d are shown in (b)–(d), respectively.

Table 3
Elemental analysis results of at the positions from No. 1 to 5 in Fig. 10(a).

Position	Element (at.%)			Phase
	Fe	Cu	Zn	
1	2.4	54.34	43.26	β-Brass
2	2.26	56.75	40.99	β-Brass
3	2.48	59.96	37.56	β-Brass
4	99.69	0.23	0.08	α-Fe
5	1.52	63.33	35.15	α-Brass

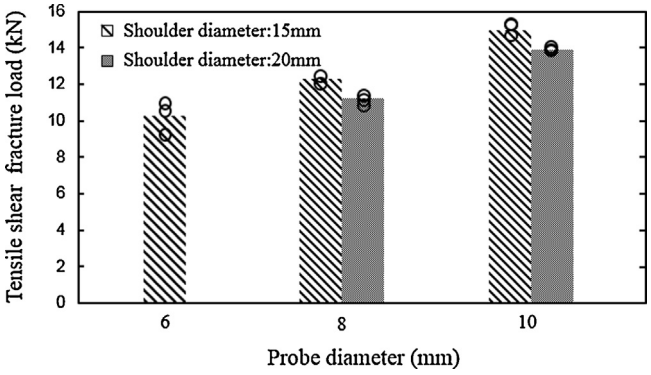

Fig. 11. Tensile shear fracture load of the lap joints with constant FSW parameters but different tools.

Fe were stirred into the brass side, and this mixing layer is about 1 μm in thickness. This is a proof that a tip of rotating probe toughed directly to the steel surface and expected to make it clean by eliminating contaminate and oxide layers. Fig. 9(a) shows the TEM BFI of the square position 1 in Fig. 8(a) and the results of line analysis of line 1 and line 2 at the interface are shown in Fig. 9(b) and (c), respectively, which shows mutual diffusion zone of Fe, Cu and Zn elements within a very narrow range of about 80 nm. Fig. 10(a) shows more higher magnification TEM micrograph of the square position 1 in Fig. 8, and Fig. 10(b)–(d) shows selected area diffraction patterns obtained from circular position b, c and d in Fig. 10(a), respectively. The dark interlayer was revealed to be β-brass. Table 3 gives the elemental analysis results at the positions from No. 1 to 5 in Fig. 10(a). Electron diffraction together with elemental analysis indicates that the dark interlayer is β-brass. No intermetallic compound was observed and detected at the interface by the analysis of selected electron diffraction patterns. This result demonstrates that the joint mechanism of brass/S25C lap joint is mutual diffusion of elements at the interface.

3.4. Tensile properties of joints

Fig. 11 shows the tensile shear test results of the joints welded with five kinds of tools. Tensile shear fracture load of the joints

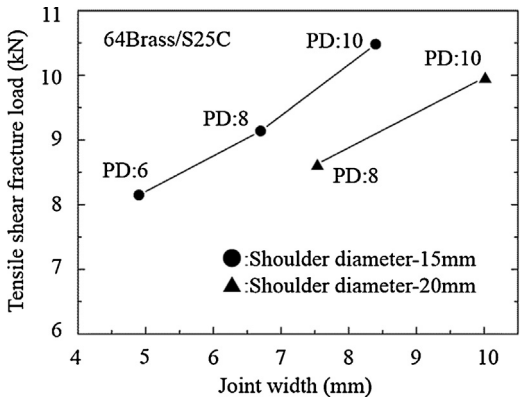

Fig. 13. Relationship between the tensile shear fracture load and the joint width.

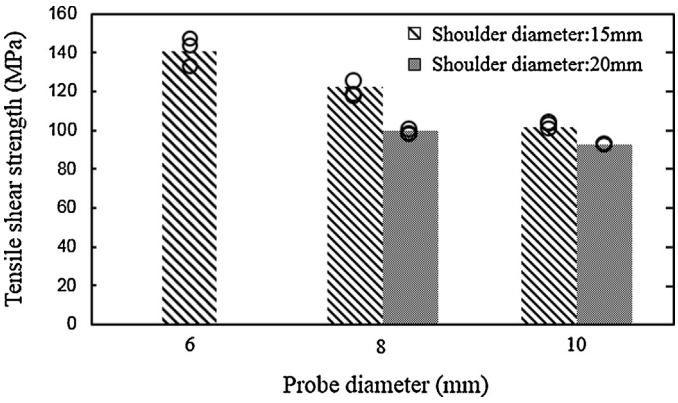

Fig. 14. Tensile shear strength of the lap joints of brass and S25C with constant FSW parameters but different tools.

increased remarkably with the increase of PD at each constant SD, but decreased slightly with the increase of SD at each constant PD of 8 and 10 mm. Fig. 12 shows the fracture surfaces of the tensile test samples and the measured values of the joint width. The joint widths were measured as the widths of the brass-adhered area on the S25C side. After tensile test, the colour of brass can be observed very clearly on the fractured surface of S25C sides. It means that most of the fractures occurred at the SZ of brass side. Fig. 13 shows the relationship between the joint width and tensile shear fracture load of the joints welded with different tools. Tensile shear fracture load increased with increasing the joint width, which was caused by the increase of PD with each constant SD, but comparing with same PD, tensile shear fracture load slightly decreased as the increase of SD in spite of the increase of the joint width. Fig. 14 shows the tensile shear strength of the joints, which was calculated by dividing the value of tensile shear fracture load with the value of joint area

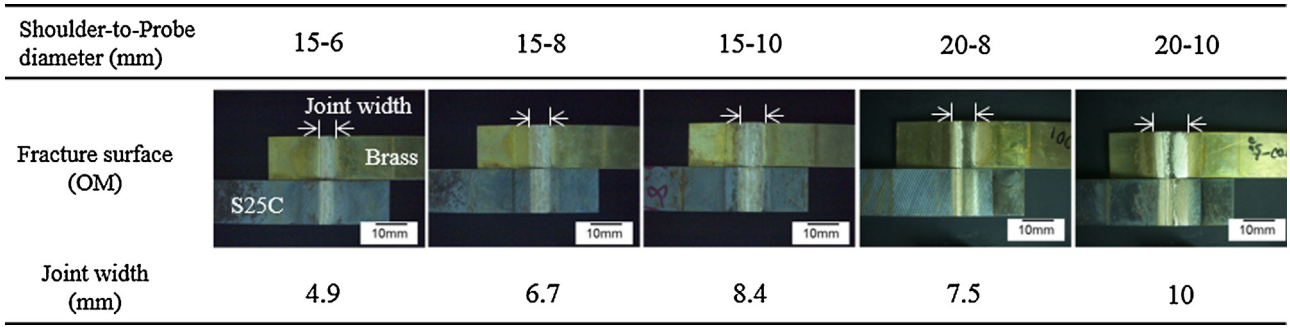

Fig. 12. Fracture surfaces of the tensile test samples and the measured valued of the joint width.

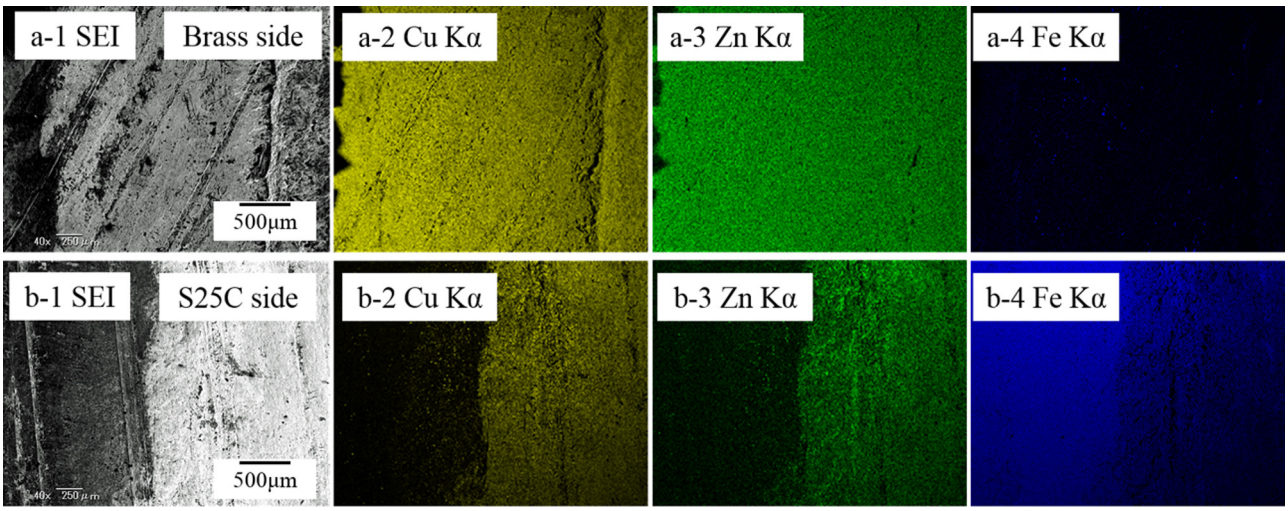

Fig. 15. The distribution of elements of the fractured surfaces of the joint welded with SD 15 mm and PD 10 mm, (a-1) and (b-1) SEM micrograph of the fractured surfaces of brass side and S25C side, (a-2) and (b-2) Cu, (a-3) and (b-3) Zn, and (a-4) and (b-4) Fe area maps, respectively.

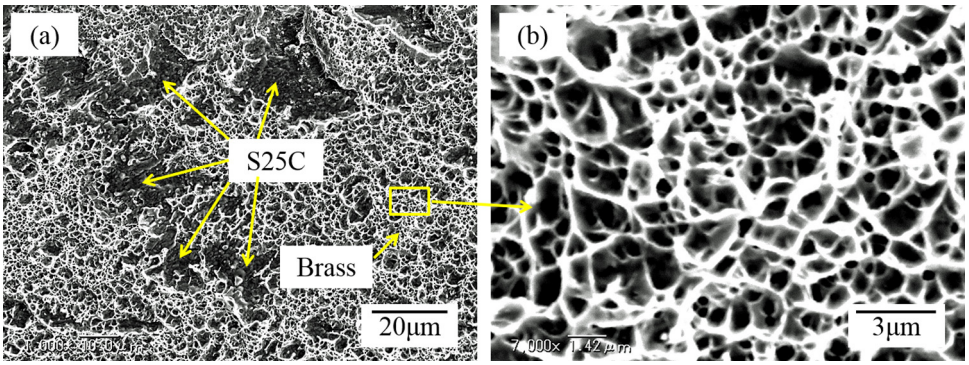

Fig. 16. SEM images of the fractured surface on the S25C side of the joint with SD 15 mm and PD 10 mm, (a) SEM image and (b) higher magnification showing dimple pattern.

(joint width × the width of tensile specimen), decreased with the increase of PD and SD.

These results demonstrates that the increase of tensile shear fracture load of the joints can be attributed to the increase of the joint width. The decrease of the tensile shear fracture load due to the increasing SD can be explained by the decrease of the strength of SZ which caused by the increase of grain size in SZ due to the increase of thermal input. The increase of PD can enlarge the joint width very directly by increasing the SZ of brass, although the increase of PD also can promoted the increase of thermal input, and therefore resulted in the decrease of the strength of the SZ. On the other hand, the increase of SD enlarged the friction surface between the shoulder and brass, and this induced more thermal input by friction and promoted the flow of brass in SZ, thus enlarged the joint width. Tensile shear strength of the joint was explained by the strength of the SZ of brass, which was closely related to the grain size of the SZ and the friction heat input at each condition of SD and PD. Joint fracture force is a function of two main factors, that is, the area and the strength of the joint interface. The increases of PD and SD showed the counter effect as the enlargement of the area but the decrease of the strength of the joint interface, respectively. Thus, as experimental result, the increase of PD proved to be more effective to the increase of the joint fracture force than the increase of SD.

Fig. 15 shows the distributions of Cu, Zn and Fe elements of the fracture surfaces of the joint with SD 15 mm and PD 10 mm. The Fe element was hardly detected at the fractured surface of brass side, but Cu and Zn as major elements of the brass were observed very clearly at the fractured surface of S25C side. Fig. 16(a) shows the SEM images of fractured surface of the S25C side, fine and uniform dimple pattern as shown in Fig. 16(b) was observed and this indicated the ductile fracture at the SZ of the brass. However, a part of fracture occurred at the interface, which were observed as black areas in Fig. 16(a), although the ratio of interface fracture zone is very small (<10%, for the whole fracture surface).

Fig. 17(a) shows the appearance of the shear tensile specimen with SD 15 mm and PD 10 mm after the shear tensile test. Bending deformation occurred for all of the shear tensile specimens and demonstrates the lap joints had certain extent of strength. Fig. 17(b) shows the cross section of the fractured surface of S25C side and a thin layer of brass was observed at the fractured surface of S25C side. The thickness of brass layer is from 1 μm to 10 μm and the brass layer is not continuous and uniform as shown in Fig. 17(c) and (d). Fig. 17(e) shows the higher magnified microstructure (SEM) of the square position e in Fig. 17(c). This phenomenon maybe can be explained by the Fe were stirred into the brass side by the FSW, and the Fe created stress concentration during the shear tensile test. Because of the distribution of Fe in the brass side is not uniform, therefore the fracture position is not fixed but near the interface.

In the usual FSW process, thermal input depended on the welding parameters (welding speed or rotation speed). Lower welding speed or higher rotation speed can increase the thermal input and then enhance the strength of lap joints within the suitable range (excess or too less thermal input can produce the lap joint gets a big burr or cannot form the joint). In this study, the effect of SD and PD on the microstructures and mechanical properties of brass/S25C lap joints was studied. As the increase of SD and PD, the thermal

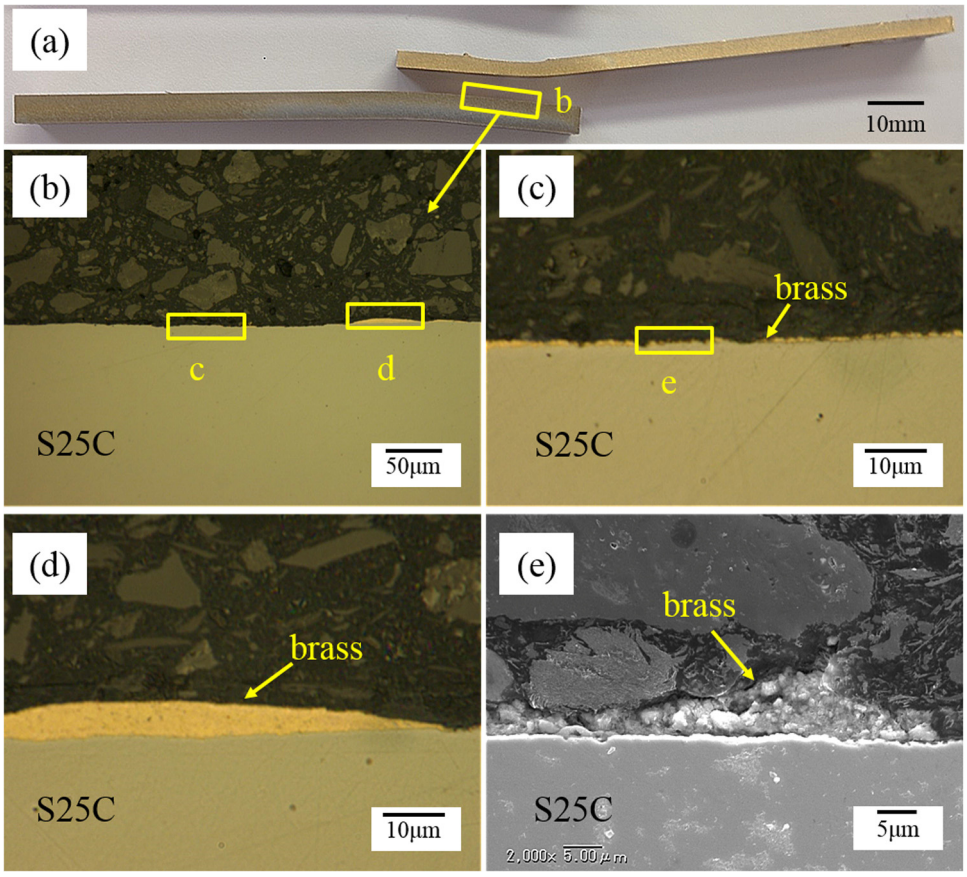

Fig. 17. Appearance of the shear tensile specimen with SD of 15 mm and PD of 10 mm after the shear tensile test and the fractured location of SZ of brass side. (a) Macroscopic picture of the shear tensile specimen, (b) cross-sections of the fractured surface on the S25C side, (c) and (d) the higher magnified image of the positions c and d are shown in (b), (e) the higher magnified image of the position e is shown in (c).

input during the FSW processes was increased and the joints got the bigger grain size, the lower hardness and the wider joint width as shown in Figs. 4 and 6. The joint strength of the joints also was enhanced via the increase of PD. All the above phenomena can be explained by the increase of thermal input (Park et al., 2004). But it is very hard to explain the decrease of joint strength with the increase of SD. Although the aforementioned statement provided one possible explanation for the phenomenon (the description for Fig. 11), but it may be explained by a new and more intuitive way.

According to the experimental results, the joint strength of FSW lap joints was improved via a bigger cleaned interface or a cleaner interface. As is well known, the front of probe contacts and cleans the surface of bottom plate during the FSW process for the lap joints. The lower welding speed or higher rotation speed of tool can provide a cleaner interface and the bigger PD can provide a bigger cleaned interface for the lap joints, therefore these methods can improve the joint strength of the lap joints. But the bigger SD cannot enlarge the cleaned interface or provide a cleaner interface, therefore the method can't improve the joint strength of the lap joints.

Based on above theory, the bigger PD can enhance the brass/steel joint strength with the constant SD and welding parameters. But the surface appearance of lap joint limits the increase of PD. If the PD becomes as big as SD, there is no shoulder to press the surface of lap joints and the surface defect (big burr or groove) will happen.

4. Conclusions

A 3.0-mm-thickness brass plate used as a top plate was lap jointed to a 5.0-mm-thickness structural steel bottom plate by friction stir welding. The effect of tool diameter on microstructure and mechanical properties of the joints was studied. The results can be summarized as follows.

1. The sound joints were achieved using the five kinds of tools with different SD and PD.
2. The tensile shear fracture load of the lap joints was remarkably improved by the increase of probe diameter, but slightly decreased with the increase of shoulder diameter. All the joints fractured at the stir zone of brass near the joint interface, and therefore the grain size of the stir zone of brass had a great influence on the performance of the joints by the Hall–Petch law. Thus, the tensile shear strength of the lap joints decreased with the increase of probe and shoulder diameters due to the increase of the grain size of the stir zone of brass.
3. A mutual diffusion zone of dominant elements of each plate was found at the interface of the joint welded by the tool with SD of 15 mm and PD of 10 mm.

References

Chen, Y.C., Nakata, K., 2008. Effect of the surface state of steel on the microstructure and mechanical properties of dissimilar metal lap joints of aluminum and steel by friction stir welding. Metall. Mater. Trans. A 39 (8), 1985–1992.
Chen, Y.C., Nakata, K., 2010. Effect of surface states of steel on microstructure and mechanical properties of lap joints of magnesium alloy and steel by friction stir welding. Sci. Technol. Weld. Joining 15 (4), 293–298.
Fujii, H., Sun, Y.F., Kato, H., Nakata, K., 2010. Materials science and engineering a-structural materials properties microstructure and processing. Mater. Sci. Eng. A 527 (15), 3386–3391.

Galvao, I., Verdera, D., Gesto, D., Loureiro, A., Rodrigues, D.M., 2013. Influence of aluminium alloy type on dissimilar friction stir lap welding of aluminium to copper. J. Mater. Process. Technol. 213 (11), 1920–1928.
Kimura, M., Kusaka, M., Kaizu, K., Fuji, A., 2010. Effect of post-weld heat treatment on joint properties of friction welded joint between brass and low carbon steel. Sci. Technol. Weld. Joining 15 (7), 590–596.
Liao, J.S., Yamamoto, N., Liu, H., Nakata, K., 2010. Microstructure at friction stir lap joint interface of pure titanium and steel. Mater. Lett. 64 (21), 2317–2320.
Luo, J., Xiang, J.F., Liu, D.J., Li, F., Xue, K.L., 2012. Radial friction welding interface between brass and high carbon steel. J. Mater. Process. Technol. 212 (2), 385–392.
Matsuyama, T., Tsumura, T., Nakata, K., 2013. Novel solid state cladding of brass to steel plate by friction stir welding. Quat. J. Jpn. Weld. Soc. 31 (4), 73–77.
Nandan, R., Debroy, T., Bhadeshia, B., 2008. Recent advances in friction-stir welding-process, weldment structure and properties. Prog. Mater. Sci. 53 (6), 980–1023.
Park, H., Kimura, T., Murakami, T., Nagano, Y., Nakata, K., Ushio, M., 2004. Microstructures and mechanical properties of friction stir welds of 60%Cu–40%Zn copper alloy. Mater. Sci. Eng. A 371 (1), 160–169.
Peel, M., Steuwer, A., Preuss, M., Withers, P.J., 2003. Microstructure, mechanical properties and residual stresses as a function of welding speed in aluminium AA5083 friction stir welds. Acta. Mater. 51 (16), 4791–4801.
Reynolds, A.P., Tang, W., 2007. Friction Stir Welding and Processing, First ed. ASM international, Ohio, pp. 15–23.